ACS APPLIED MATERIALS & INTERFACES

Research Article

www.acsami.org

Morphology Control in the Synthesis of $CaCO_3$ Microspheres with a Novel CO_2-Storage Material

Tianxiang Zhao, Bo Guo, Fei Zhang, Feng Sha, Qiang Li, and Jianbin Zhang*

College of Chemical Engineering, Inner Mongolia University of Technology, Huhhot 010051, China

Supporting Information

ABSTRACT: A green and template-free method was applied to control the morphology of $CaCO_3$ microspheres with a layered nanostructure surface and pure crystalline phase of vaterite via the hydrothermal reaction between $Ca(OH)_2$ saturated limpid solution and a novel CO_2-storage material (CO_2SM). Morphologies of the as-prepared $CaCO_3$ crystals could be tuned with CO_2SM concentration, reaction temperature, or crystallization time. After the precipitation of $CaCO_3$ crystals, the filtered solution could not only be used to absorb CO_2 but also to produce $CaCO_3$ microspheres repeatedly with the addition of $Ca(OH)_2$ solution. Furthermore, an aggregation and self-assembly mechanism for the formation $CaCO_3$ microspheres had been proposed. As a result, this novel synthesis strategy of $CaCO_3$ microspheres with CO_2SM again emphasized that was possible to synthesize inorganic/organic hybrid materials with exquisite morphology and offered an alternative way for comprehensive utilization of CO_2.

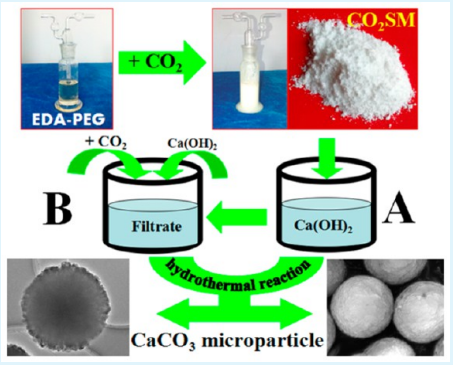

KEYWORDS: *calcium carbonate, CO_2-storage materials, microspheres, morphology control, mineralization, CO_2 capture and utilization*

1. INTRODUCTION

Carbon dioxide (CO_2), a greenhouse gas, is related to a series of environmental changes. In an attempt to mitigate these environmental changes, many researchers have focused on technologies to capture and control anthropogenic CO_2.[1,2] To reduce CO_2 emissions, various methods,[3−5] including absorption, adsorption, hydrate-based separation processes, and disposal of CO_2 in deep oceans, have been developed for CO_2 capture and storage (CCS) processes. However, all current CCS approaches have critical drawbacks, i.e., leaking of CO_2 from storage sites to land surface, large amounts of byproduct, high cost, slow carbonation rate, and noneffective CO_2 utilization.[6,7] Compared with CCS, CO_2 capture, utilization, and storage (CCUS) approaches are more attractive than CCS because they can not only consume CO_2 but also produce value-added chemicals.[8−11]

In the sequestration of CO_2 into mineral carbonates with aqueous saturated CO_2 solutions,[12−14] it is well-known that carbonation can be promoted by amine-containing chemicals, such as aqueous ethanediamine (EDA)[5] and monoethanolamine (MEA),[6] with characteristic absorption abilities toward acidic CO_2 gas. Recently, CO_2 has been mineralized into different $CaCO_3$ polymorphs and morphologies in an aqueous amine−CO_2 system[15−18] with different additives and soft templates[19,20] because $CaCO_3$ is not only one of the most abundant mineral materials in nature but also has great potentials in paints, paper, plastics, rubber, and fabrication of biomimetic materials.[21−23] For example, inspired by nature, biomimetic $CaCO_3$ crystals have been successfully synthesized through reverse microemulsion or complex micelle,[24] hydrogels,[25] self-assembled monomolecular (SAM) films,[26] Langmuir monolayers[27] and double hydrophilic block copolymers (DHBCs).[28,29] However, CO_2-storage material (CO_2SM), which is product of equimolar EDA and polyethylene glycol 300 (PEG) with CO_2, has not been used to produce $CaCO_3$ crystal up to present.

Herein, we reported a novel and template-free method to control the morphology of $CaCO_3$ microspheres during synthesis from CO_2SM and $Ca(OH)_2$-saturated limpid solution (Figure 1). Additionally, after synthesis the filtered solution without $CaCO_3$ precipitate could be recycled and used to prepare $CaCO_3$ microspheres repeatedly.

2. EXPERIMENTAL SECTION

2.1. Materials. Analytical-grade EDA was purchased from Tianjin Reagent Company. Analytical-grade polyethylene glycol 300 (PEG) with the average molecular weight of 300 (280−310) was purchased from Beijing Reagent Company. Compressed CO_2 (99.999% vol) was purchased from the Standard Things Center (China). $Ca(OH)_2$ was purchased from Sinopharm Chemical Reagent Co., Ltd. For synthesis method and information on CO_2SM, refer to the Supporting Information (Figures S1−S3) and our most recent work.[30]

2.2. Synthetic Procedures. The crystallization of $CaCO_3$ was carried out hydrothermally at T = 60−120 °C with 50 mL of $Ca(OH)_2$-saturated limpid solution. Typically, approximately 5.0 g of CO_2SM was mixed with $Ca(OH)_2$-saturated solution first, then the mixture was transferred into a 100 mL Teflon-lined stainless-steel

Received: April 24, 2015
Accepted: July 1, 2015
Published: July 15, 2015

DOI: 10.1021/acsami.5b03568
ACS Appl. Mater. Interfaces 2015, 7, 15918−15927

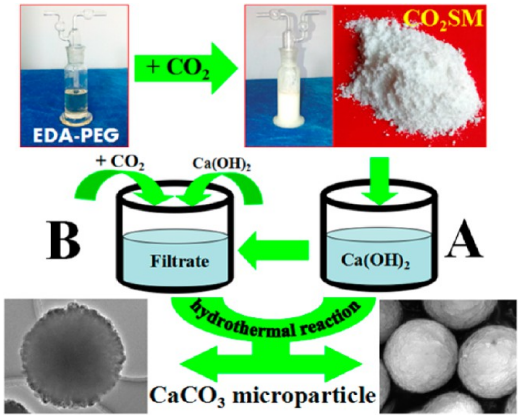

Figure 1. Morphology control in the synthesis of $CaCO_3$ microspheres using CO_2SM. A and B represent the hydrothermal reactor. In the processes, the filtered solution without $CaCO_3$ precipitate can not only repeatedly absorb CO_2 but also recycle to produce $CaCO_3$ microspheres after bubbling CO_2. This cycle of absorption of CO_2 for preparing calcium carbonate is a process that could potentially be optimized as a novel technique.

hydrothermal reactor. The reactor was sealed tightly and heated at 90 °C for 2 h. The as-obtained precipitate was separated with vacuum filtration and washed with double-distilled water and ethanol. The as-synthesized $CaCO_3$ powder was dried under vacuum at 120 °C for 8 h. In particular, all $CaCO_3$ samples were prepared in the same way.

2.3. Characterization. Morphologies of the synthesized $CaCO_3$ particles were examined via scanning electron microscopy (SEM, Quanta FEG 650, China) with an accelerating voltage of 20 kV and high-resolution transmission electron microscope (HR-TEM, JEM-2100, Japan) with an accelerating voltage of 200 kV. The energy dispersive X-ray (EDX) method was employed to confirm the chemical composition of $CaCO_3$ particles. X-ray diffraction (XRD) patterns were collected on a powder X-ray diffractometer (Siemens D/max-RB) with Cu Kα radiation and a scanning rate of 0.05°·s^{1-}.

The relative percentage of each polymorph of $CaCO_3$ was calculated from their characteristic XRD peak intensities according to the following equations.[31]

$$X_V = \frac{7.691(I_V^{110})}{I_C^{104} + 7.691(I_V^{110}) + 3.157(I_A^{221})} \quad (1)$$

$$X_V + X_A + X_C = 1.0 \quad (2)$$

$CaCO_3$ samples containing only vaterite and calcite were analyzed by the following set of equations.

$$\frac{I_C^{104}}{I_V^{110}} = 7.691\frac{X_C}{X_V} \quad (3)$$

$$X_C + X_V = 1.0 \quad (4)$$

where X_V, X_A, and X_C are the molar fraction of vaterite, aragonite and calcite, respectively. Peak intensities of 110 plane (I_V^{110}), 221 plane (I_A^{221}), and 104 plane (I_C^{104}) represent vaterite, aragonite and calcite, respectively.

FTIR was recorded on a Nexus 670 infrared spectrophotometer. Thermogravimetric analysis (TGA, Entzsch-Sta 449) was employed to measure the weight percentage of the CO_2SM and $CaCO_3$ precipitate. Nitrogen sorption data were recorded on a Tristar II3020 automated gas adsorption analyzer. Isotherms were evaluated with the BJH theory to give the pore parameters, such as BET surface areas, pore volume, and pore size distribution.

3. RESULTS AND DISCUSSION

][

3.1. Effect of CO_2SM Concentration on Crystallization of $CaCO_3$. Morphologies of $CaCO_3$ crystals with different CO_2SM concentrations (Table 1) were characterized by SEM, XRD, and FTIR.

According to SEM images in Figure 2, CO_2SM concentration had a significant influence on $CaCO_3$ morphology. The $CaCO_3$ precipitates have littery morphologies. With the increase of CO_2SM concentration, the morphology of $CaCO_3$ precipitate gradually changed from littery (rhombohedra (marked by an arrow), spherical or spheroidicity, cubical, baculiform, laminated cubed shape, layered porous hierarchical structures, thin pancake sample, needlelike, and complex crystal) to microsphere morphologies with a size range of 2.4−5.6 μm. These results suggested that CO_2, PEG, and EDA concentrations from CO_2SM were indispensable and cooperatively help $CaCO_3$ grow along the same direction, in which PEG could be considered as a cosolvent and EDA might be used to adjust the pH value of the reaction system.

Figure 3 shows XRD and FTIR of as-prepared $CaCO_3$ precipitates synthesized with different concentration of CO_2SM. According to XRD results, the crystalline phase of $CaCO_3$ in sample A precipitate was pure calcite, and samples B−E were mixed calcite and vaterite. The relative percentages of each crystalline phase of $CaCO_3$ were calculated and are listed in Table 1 and Figure S4. In Table 1, a low concentration of CO_2SM was usually accompanied by a lower pH value and favored the formation of calcite. With the increase of CO_2SM concentration and pH value, the tendency to form calcite declined. When CO_2SM concentration was greater than or equal to 10 g·L^{-1}, a mixed crystalline phase of calcite and vaterite was obtained. Here, the crystallization of $CaCO_3$ was influenced by CO_2SM concentration because the produced PEG and EDA molecules from CO_2SM decomposition could

Table 1. $CaCO_3$ Samples Prepared under Different CO_2SM Concentrations at T = 100 °C and t = 1 h and Experimental Conditions, Polymorph Compost, and Primary Morphologies for Each Sample

		polymorph compost (%)[c]			
samples[a]	preparation conditions[b]	calcite	aragonite	vaterite	primary morphologies
A	CO_2SM (4 g·L^{-1}); pH 8.0	100	0	0	irregular
B	CO_2SM (10 g·L^{-1}); pH 8.5	89.9	0	10.1	irregular
C	CO_2SM (20 g·L^{-1}); pH 9.6	57.67	0	42.33	irregular and spherical
D	CO_2SM (40 g·L^{-1}); pH 10.4	49.78	0	50.22	irregular and spherical
E	CO_2SM (70 g·L^{-1}); pH 12.5	45.80	0	54.20	spherical
F	CO_2SM (100 g·L^{-1}); pH 13.3	34.59	0	65.41	spherical

[a]In all cases, 50 mL of $Ca(OH)_2$ saturated limpid solution was used. [b]Concentration (g·L^{-1}) of CO_2SM was calculated as milligrams of CO_2SM dispersed in 50 mL of $Ca(OH)_2$ saturated limpid solution; the reaction time and temperature are 1 h and 100 °C, respectively. [c]Calculated from the XRD pattern.

DOI: 10.1021/acsami.5b03568
ACS Appl. Mater. Interfaces 2015, 7, 15918−15927

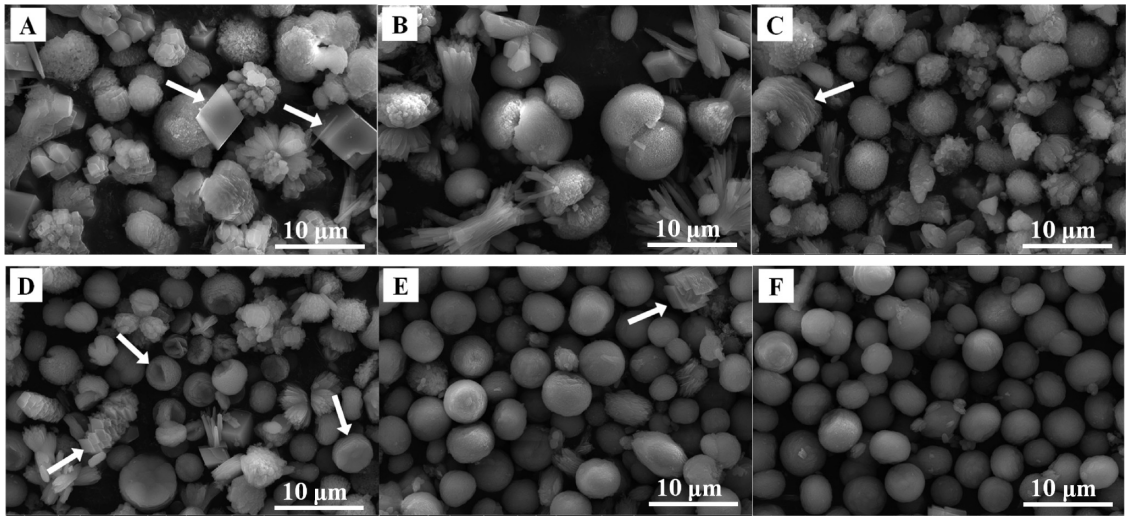

Figure 2. SEM micrographs of $CaCO_3$ samples were acquired under different concentrations of CO_2SM at 100 °C for 1 h. Concentrations of CO_2SM are sample A, 4 g·L^{-1}; sample B, 10 g·L^{-1}; sample C, 20 g·L^{-1}; sample D, 40 g·L^{-1}; sample E, 70 g·L^{-1}; and sample F, 100 g·L^{-1}.

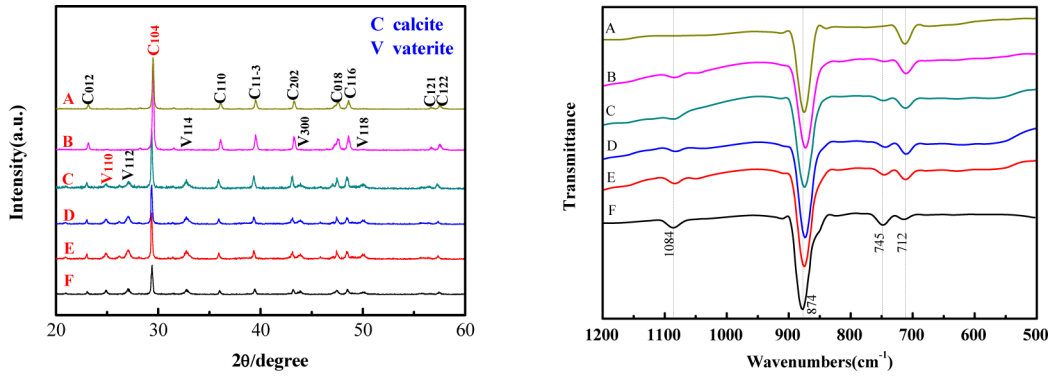

Figure 3. XRD patterns and segmented FTIR spectra of the $CaCO_3$ samples were obtained with different concentrations of CO_2SM at 100 °C for 1 h. Concentrations of CO_2SM are sample A, 4 g·L^{-1}; sample B, 10 g·L^{-1}; sample C, 20 g·L^{-1}; sample D, 40 g·L^{-1}; sample E, 70 g·L^{-1}; and sample F, 100 g·L^{-1}.

serve as block copolymer templates or structure-directing agents and EDA could adjust the pH value of the reaction system to influence crystallization of $CaCO_3$.[32−35] SEM and XRD also showed clearly that the particle had either a pure calcite phase or a mixed crystalline phase of calcite and vaterite.

Usually, the characteristic FTIR absorption bands of C−O bond vibrations of $CaCO_3$[36−38] include symmetric stretching (υ_1 mode), out-of-plane bending (υ_2 mode), doubly asymmetric stretching (υ_3 mode), and doubly in-plane bending (υ_4 mode). The characteristic carbonate infrared vibrations for pure calcite and mixed crystalline phase of calcite with vaterite are shown in Figure 3. Sample A had three characteristic peaks at 1084, 874, and 712 cm^{-1} (υ_4 mode of calcite), which indicated the pure calcite phase. With the increase of CO_2SM concentration, a new peak appeared gradually at 745 cm^{-1} (υ_4 mode of vaterite), which indicated the mixed phase of calcite and vaterite in samples B−E.[36] Additionally, the peak intensity at 712 cm^{-1} decreased with the gradual appearance of the 745 and 1084 cm^{-1} peaks, probably because the formation of thermodynamically most stable calcite phase was restrained and the mixed crystalline phase of calcite and vaterite was promoted, which agreed well with the XRD data.

3.2. Effect of Reaction Temperature on Crystallization of $CaCO_3$. As shown in Figure 4, reaction temperature had a great influence on the morphology of the as-prepared $CaCO_3$ crystal, and the preparation conditions are listed in Table 2. In sample A, except for a $CaCO_3$ sphere, inhomogeneous $CaCO_3$ particulate with flowerlike and/or rodlike shapes and unusual dendritelike crystals with a diameter of about 10−15 μm were formed, in which the dendritelike crystal had joined parts from multiple rodlike shape crystals with a diameter of 3.5 μm. In samples B and C, a rodlike shape and defective spheres of $CaCO_3$ with uneven sizes were formed. Surfaces of these defective spheres were composed of plentiful nanoparticles. A similar result was found in sample D. In sample E, the surface of the microsphere became close-knit when the reaction temperature was 120 °C. With the increase of temperature, the average diameter of these microspheres was gradually increased, and the crystallization of $CaCO_3$ morphologies trended toward a consistent direction. Samples F−H showed the influence of the temperature on the morphologies, size, and size distribution of $CaCO_3$ crystal with a relatively high concentration of CO_2SM (100 g·L^{-1}) and high pH (13.3). In particular, the pH of solution also observably influences crystallization of $CaCO_3$.[39] For samples F−H, pH of the solution was relatively far from the isoelectric point of $CaCO_3$, which is pH 9.5 according to the literature.[40] The fine crystalline $CaCO_3$ particles from the primary nucleation might coagulate each other because of the strong electrostatic repulsive force between them. The most interesting feature was that $CaCO_3$

DOI: 10.1021/acsami.5b03568
ACS Appl. Mater. Interfaces 2015, 7, 15918−15927

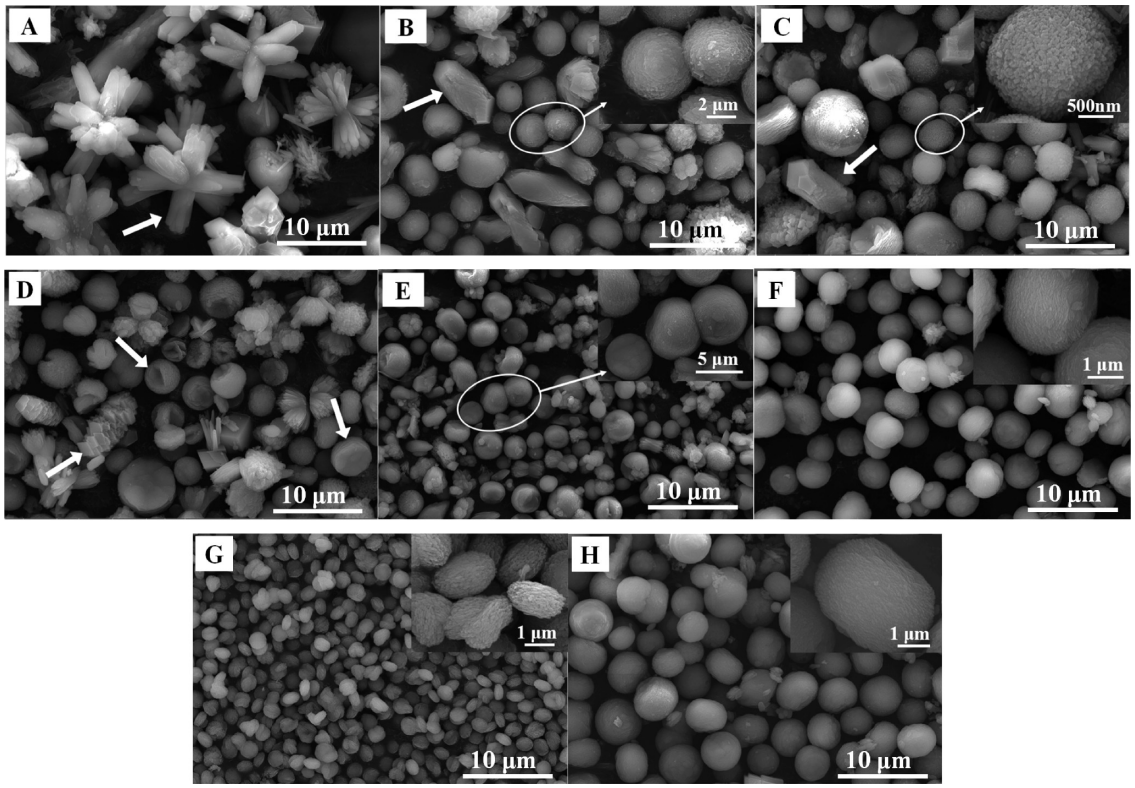

Figure 4. SEM micrographs of $CaCO_3$ samples were acquired under different temperatures for 1 h. When the concentration of CO_2SM is 40 g·L^{-1}, the reaction temperatures are sample A, 60 °C; sample B, 80 °C; sample C, 90 °C; sample D, 100 °C; and sample E, 120 °C. When the concentration of CO_2SM is 100 g·L^{-1}, the reaction temperatures are sample F, 80 °C; sample G, 90 °C; and sample H, 100 °C.

Table 2. $CaCO_3$ Samples Prepared under Different Reaction Temperatures at t = 1 h and Experimental Conditions, Polymorph Compost, and Primary Morphologies for Each Sample

		polymorph compost[c]			
samples[a]	preparation conditions[b]	calcite	aragonite	vaterite	primary morphologies
A	pH 10.4; T = 60 °C	42.0	9.00	49.0	flowerlike shape
B	pH 10.4; T = 80 °C	10.0	9.18	80.8	irregular, spherical and rodlike shape
C	pH 10.4; T = 90 °C	0	0	100	irregular, spherical and rodlike shape
D	pH 10.4; T = 100 °C	49.78	0	50.22	irregular and spherical
E	pH 10.4; T = 120 °C	100	0	0	irregular, and spherical
F	pH 13.3; T = 80 °C				spherical
G	pH 13.3; T = 90 °C	0	0	100	spheroidicity
H	pH 13.3; T = 100 °C	34.59	0	65.41	spherical

[a]In all cases, 50 mL of $Ca(OH)_2$ saturated limpid solution was used, and the concentration of CO_2SM in samples A–E is 40 g·L^{-1}, and in samples F–H, it is 100 g·L^{-1}. The reaction times are 1 h. [b]Standard uncertainties u for each variables are $u(T)$ = 1 K. [c]Calculated from the XRD pattern.

crystals with spheroidicity morphologies were synthesized at 90 °C with a size of 1.0 μm × 1.7 μm (sample G). Simultaneously, spherical $CaCO_3$ particles were obtained when reaction temperatures were 80 and 100 °C (samples F and H, respectively), but these $CaCO_3$ microspheres have a pyknotic surface and larger diameter of 2.5–5.1 μm. Some individual $CaCO_3$ particles (Figure S5) could also be obtained at low reaction temperatures (T < 70 °C) with low CO_2SM concentration (pH ≤8.5). These results suggested that low reaction temperature and a low pH that was relatively far from the isoelectric point of $CaCO_3$ were conducive to the formation of polymorphous $CaCO_3$, whereas the increase of reaction temperature promoted the formation of $CaCO_3$ with unified microspheres.

XRD and FTIR data of as-prepared $CaCO_3$ precipitates are shown in Figure 5. The relative percentages of each crystalline phase calculated from their characteristic XRD peaks intensities are shown in Table 2 and Figure S6. Three crystalline phases of $CaCO_3$, including calcite, aragonite, and vaterite, were formed at 60 and 80 °C; the increased vaterite phase and decreased calcite phase were found when the reaction temperature was changed from 60 to 90 °C, which indicated that the low temperature was beneficial to the coexistence of all the three of crystal phases. Pure vaterite phase was formed when the reaction temperature was 90 °C, probably because the decomposition of CO_2SM was remarkable at approximately 90 °C. However, with the further increase of temperature, the crystalline phase of vaterite was gradually decreased, and rhombohedral calcite was increased. These XRD results were further reconfirmed by FTIR data. As shown in Figure 5, samples A and B had four peaks at 1083, 875, 745, and 712 cm^{-1}. The vibration bands at 1083, 875, and 745 cm^{-1} could be

DOI: 10.1021/acsami.5b03568
ACS Appl. Mater. Interfaces 2015, 7, 15918–15927

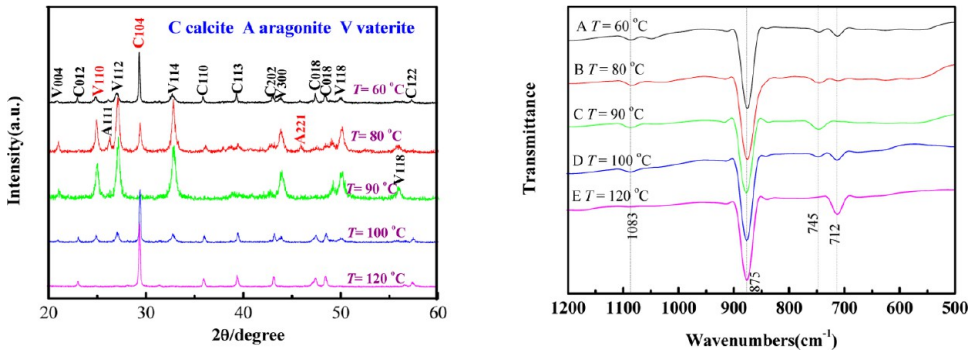

Figure 5. XRD patterns and segmented FTIR spectra of $CaCO_3$ samples were obtained with different reaction temperatures and a constant concentration of the CO_2SM for 1 h. When the concentration of CO_2SM is 40 g·L^{-1}, the reaction temperatures are sample A, 60 °C; sample B, 80 °C; sample C, 90 °C; sample D, 100 °C; and sample E, 120 °C. When the concentration of CO_2SM is 100 g·L^{-1}, the reaction temperatures are sample F, 80 °C; sample G, 90 °C; and sample H, 100 °C.

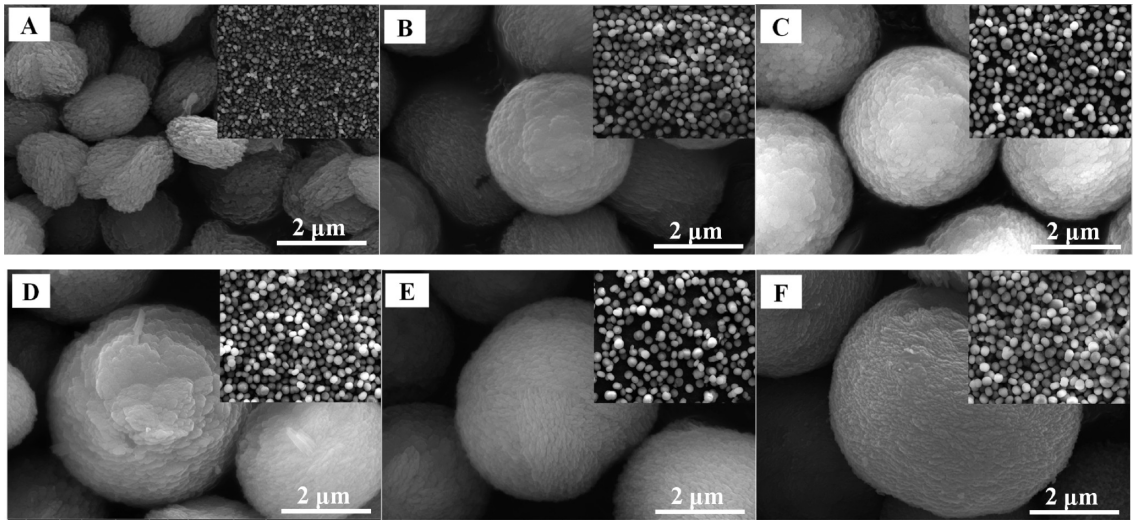

Figure 6. SEM micrographs of $CaCO_3$ samples acquired under different reaction times at 90 °C. When the concentration of CO_2SM is 100 g·L^{-1}, the reaction times are sample A, 1 h; sample B, 2 h; sample C, 4 h; sample D, 6 h; sample E, 8 h; and sample F, 10 h.

Table 3. $CaCO_3$ Samples Prepared under Different Reaction Time at T = 90 °C and Experimental Conditions, Polymorph Compost, and Primary Morphologies for Each Sample

		polymorph compost[c]			
samples[a]	preparation conditions[b]	calcite	aragonite	vaterite	primary morphologies
A	pH 13.3; t = 1 h	0	0	100	spheroidicity
B	pH 13.3; t = 2 h	0	0	100	spherical
C	pH 13.3; t = 4 h	1.90	0	98.1	spherical
D	pH 13.3; t = 6 h	2.72	0	97.28	irregular or defective balls
E	pH 13.3; t = 8 h	5.01	0	94.99	irregular or defective balls
F	pH 13.3; t = 10 h	8.27	0	91.73	irregular or defective balls

[a]In all cases, 100 g·L^{-1} CO_2SM was calculated as milligrams of CO_2SM dispersed in 50 mL of $Ca(OH)_2$ saturated limpid solution. [b]The reaction temperatures are 90 °C. [c]Calculated from the XRD pattern.

assigned to the characteristic vibrations of vaterite, and 712 cm^{-1} could be due to the characteristic vibration of calcite.[37,38] However, infrared characteristic absorption peak of aragonite at about 854 cm^{-1} was not found because the aragonite content was limited. Sample C has three vibration bands at 1083, 875, and 745 cm^{-1}, which confirmed the presence of vaterite.[37,38] Sample E also has three peaks at 1083, 875, and 712 cm^{-1}, which confirmed the presence of calcite.[37,38] Sample D, in addition to peaks at 1083 and 875 cm^{-1}, had peaks at 745 and 712 cm^{-1} (υ_4 mode of vaterite and υ_4 mode of calcite, respectively), which confirmed the presence of calcite along with vaterite.[37,38] These FTIR results also proved that the $CaCO_3$ samples with different crystalline phase were in good agreement with their XRD results.

In this study, CO_2SM could not only release CO_2 to the crystallization solution when the system temperature is higher than the decomposition temperature of CO_2SM but also could produce EDA and PEG to control the crystallization of $CaCO_3$. At 60 °C, CO_2SM could not release CO_2, so alkyl carbonate ion ($R\text{-}CO_3^-$) was likely formed through the hydrolysis of CO_2SM

DOI: 10.1021/acsami.5b03568
ACS Appl. Mater. Interfaces 2015, 7, 15918−15927

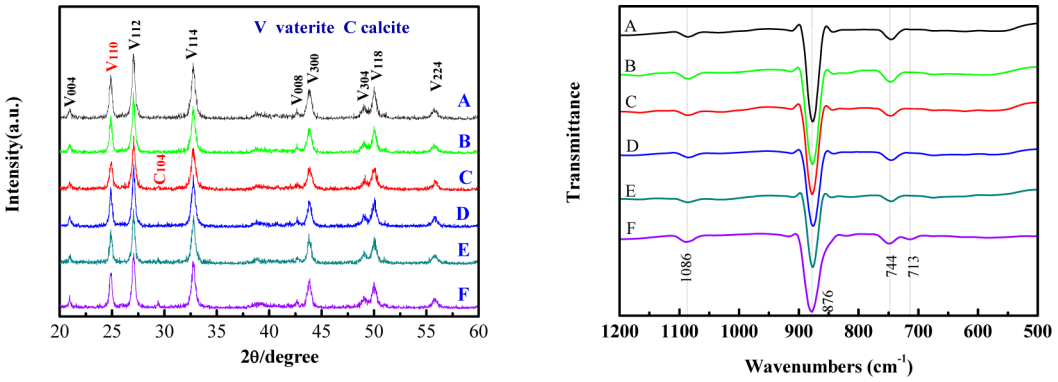

Figure 7. XRD patterns and segmented FTIR spectra of $CaCO_3$ samples were obtained with different reaction times at 90 °C and a constant concentration of the CO_2SM (100 g·L^{-1}. The reaction times are sample A, 1 h; sample B, 2 h; sample C, 4 h; sample D, 6 h; sample E, 8 h; and sample F, 10 h.

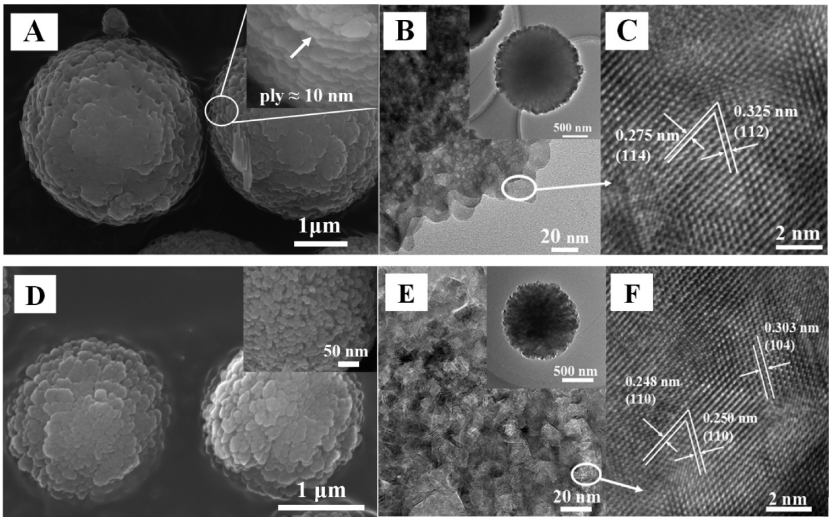

Figure 8. Electron microscopy micrographs of $CaCO_3$ samples acquired. (A) no heat treatment, (B) TEM of A, (C) HR-TEM of A, (D) heat treated, (E) TEM of D, and (F) HR-TEM of D.

to produce $CaCO_3$ precipitate, although further studies are needed to establish the mechanism of $CaCO_3$ crystallization.

3.3. Effect of Reaction Time on Crystallization of $CaCO_3$. Representative SEM images of the as-prepared $CaCO_3$ precipitates were presented in Figure 6, and the preparation conditions and primary morphologies of each sample were listed in Table 3. As shown in Figure 6, the $CaCO_3$ crystal gradually changed from the initial spheroidicity to a sphere. However, with the extension of reaction time, these microspheres continued to grow and eventually formed irregular or defective balls with a larger average diameter, and the surfaces of these particles were changed significantly from incompact to compact.

As shown in Figure 7 of XRD, the pure vaterite phase was formed when the reaction time was 1 h (sample A) and 2 h (sample B); three characteristic peaks at 1083, 875, and 745 cm^{-1} were detected for samples A and B, which indicated that vaterite was formed.[37,38] When the reaction time was increased to 4 h, the crystalline phase of calcite began to appear, although the $CaCO_3$ samples were composed of vaterite and only a little calcite. The relative percentage of each crystalline phase was calculated from their characteristic XRD peak intensities, and the results are shown in Table 3 and Figure S7. With the further extension of reaction time, most crystalline $CaCO_3$ phase was still vaterite, indicating that the reaction time mainly affected the sizes and surface structure of $CaCO_3$ microspheres rather than its composition. Furthermore, the FTIR results showed a decrease of intensity at 745 cm^{-1} and the gradual appearance of a peak at 713 cm^{-1}, which indicated that the most thermodynamically unstable vaterite phase gradually disappeared and a mixture of vaterite and calcite phases formed.

3.4. Properties of $CaCO_3$ Microspheres. To feature the multihole structure of $CaCO_3$ microparticles and study their crystalline phase transformation and compositions, properties of $CaCO_3$ microspheres before and after high-temperature annealing treatment at 400 °C for 5 h were compared. As shown in Figure 8A, the layered and scobinate spherical $CaCO_3$ particles were formed with a mean diameter of around several micrometers; the large sphere particles seemed to be formed through an ordered overlapping of many flakes with average thickness of approximately 10 nm. As shown in Figure 8D, the heat-treated $CaCO_3$ microspheres had a more prominent porous structure and rough surface than those of no-heat-treatment microspheres (Figure 8D); more importantly, their surface became more decompacted than that of no-heat-treatment microspheres, which was due to the loss of samples with relatively poor thermostability such as water, EDA, and PEG and materials exposed after high-temperature annealing

DOI: 10.1021/acsami.5b03568
ACS Appl. Mater. Interfaces 2015, 7, 15918−15927

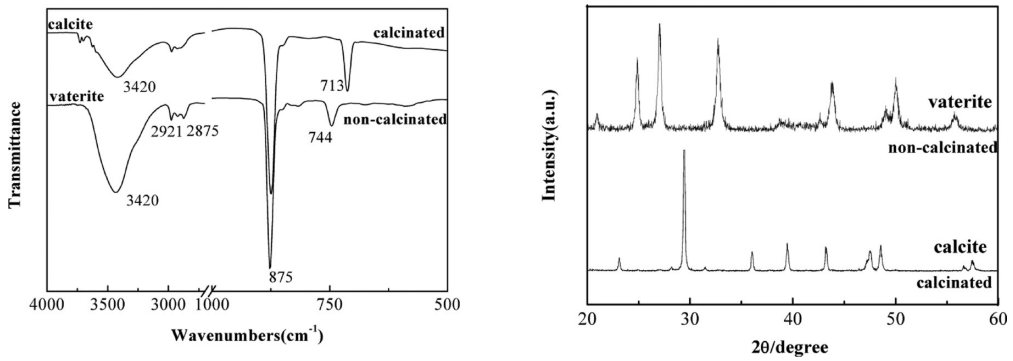

Figure 9. FTIR spectra and XRD patterns of the $CaCO_3$ microspheres before and after heat treatment.

treatment. Furthermore, EDX (Figure S8) showed that $CaCO_3$ particles only contained carbon, calcium, and oxygen. Other elements such as nitrogen and hydrogen from EDA or PEG have not been found because these element contents were limited in the as-prepared $CaCO_3$.

SEM images showed that the surface of $CaCO_3$ microspheres was compact before high-temperature annealing treatment (Figure 8A), and the unconsolidated surface of $CaCO_3$ microspheres could be found after high-temperature annealing treatment (Figure 8D). TEM results also confirmed that the more significant pore structure of the heat-treated $CaCO_3$ microspheres (Figure 8B) compared with that of the no-heat-treatment sample (Figure 8E). BET measurement (Figure S9) of no-heat-treatment $CaCO_3$ sample showed that the surface area and the pore diameter were 33.32 $m^2 \cdot g^{-1}$ and 11.32 nm, respectively. By contrast, the BET surface area was dramatically increased to 97.54 $m^2 \cdot g^{-1}$ with average pore size of 28.24 nm after the as-prepraed $CaCO_3$ sample was treated at 400 °C for 5 h, probably because pores of $CaCO_3$ were filled with water and organic compound, such as EDA and PEG, and high-temperature annealing treatment made the pore structure become more remarkable. The thermogravimetric data (Figure S10) confirmed the presence of water or organics in $CaCO_3$ sample before high-temperature annealing, in which the first stage was from room temperature to 570 °C with a mass loss of approximately 3.5% caused by the evaporation of physically and chemically absorbed water or organic compounds and the second endothermic stage was at about 732 °C because of the thermal decomposition of $CaCO_3$ ($CaCO_3 \rightarrow CaO + CO_2 \uparrow$).[41] Inversely, only a stage of weight loss of $CaCO_3$ microspheres after high-temperature annealing treatment, indicating that water or organic compounds in $CaCO_3$ samples were dislodged when $CaCO_3$ sample was heated at 400 °C for 5 h. As shown in the FTIR data in Figure 9, nonsymmetrical and symmetrical stretching vibrations of C−H ($-CH_2-$) of PEG or EDA at 2974 and 2875 cm^{-1}, respectively,[23,42] and the broad peaks of the stretching vibration of O−H from water and PEG at around 3420 cm^{-1} were found in as-made $CaCO_3$,[43] indicating that the as-prepared products contained not only $CaCO_3$ crystals but also organic molecules and water. However, the characteristic vibration band of $-CH_2-$ did not completely disappear after high-temperature annealing treatment, and the intensity of the stretching vibration of O−H became weaker, indicating that segmental organics and crystal water in $CaCO_3$ crystals the high-temperature annealing treatment.

According to the comparison of XRD patterns and FTIR (Figure 9) of $CaCO_3$ microspheres before and after high-temperature annealing treatment, the high-temperature annealing treatment obviously influenced the crystalline phase of $CaCO_3$ microspheres with the polymorph transformations of $CaCO_3$ microspheres.[44] As shown in HR-TEM images of $CaCO_3$ microsphere (Figure 8C), a (114) plane with a lattice of 0.275 nm and a (112) plane with a lattice spacing of 0.325 nm were found, which could be assigned to crystal lattice of the vaterite.[45] The lattice distances of $CaCO_3$ microsphere with high-temperature annealing treatment were 0.248, 0.250, and 0.303 nm, in which the first and second were from the (110) plane of calcite and the third was due to the (104) plane (Figure 8F).[46,47] These HR-TEM results suggested that the high-temperature annealing treatment could make crystalline-phase $CaCO_3$ microspheres change from vaterite to calcite.

3.5. Possible Formation Mechanism of $CaCO_3$ Microspheres. In this study, aggregates of PEG and EDA[33−35,48] in aqueous should be similar to a surfactantlike structure that was the template to adjust the crystallization of $CaCO_3$, and a possible formation mechanism of $CaCO_3$ microspheres was shown in Figure 10.

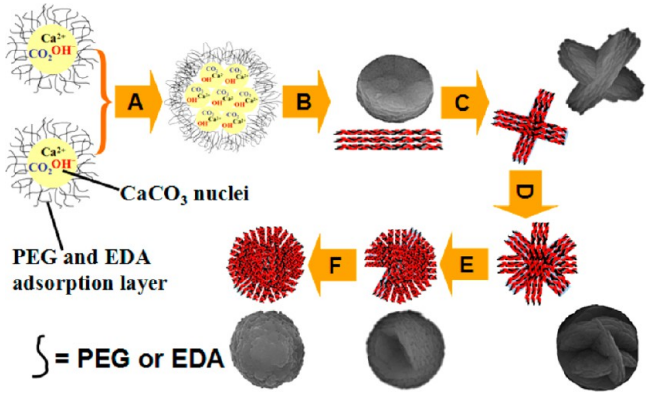

Figure 10. Schematic illustration of the possible formation process of $CaCO_3$ microspheres with porous surface textures formed at 90 °C for 2 h. A: heterogeneous nucleation processes to form $CaCO_3$ preliminary nanoparticles; B: formation of aggregated flake or pancake structures; C: formation of decussate structures; D: assembly into a defective $CaCO_3$ microsphere; E: further growth of defective spherical $CaCO_3$ particles; and F: assembly into a complete microsphere.

In this mechanism, PEG and EDA would play crucial roles in the formation of $CaCO_3$ crystals with EDA as pH-adjusting agent and PEG as cosolvent to adjust the crystallization of $CaCO_3$. Additionally, the lone-pair electrons on the oxygen atoms in PEG and nitrogen atoms in EDA could be not ignored because of strong electrostatic interactions between PEG (and/

DOI: 10.1021/acsami.5b03568
ACS Appl. Mater. Interfaces 2015, 7, 15918−15927

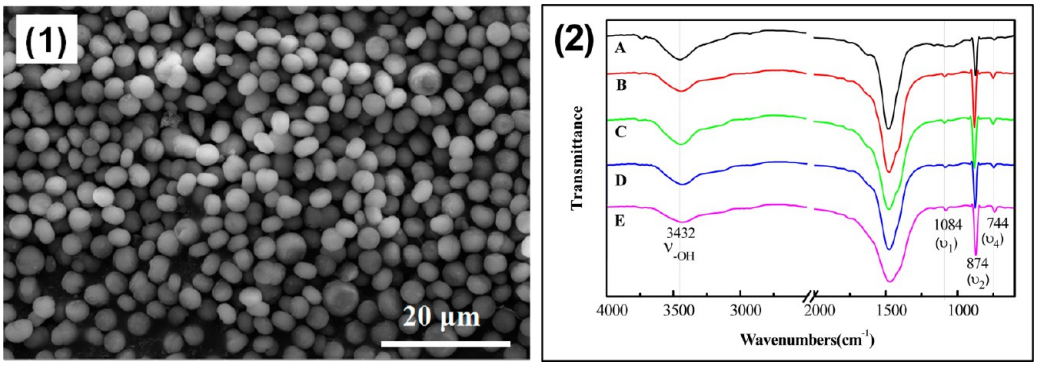

Figure 11. (1) SEM picture of $CaCO_3$ microspheres is acquired for the first time cycle, and other SEM micrographs of $CaCO_3$ microspheres are presented in Figure S13; (2) FTIR spectra of $CaCO_3$ microspheres were acquired after five cycles, and (A–E) represent the number of experiments.

or EDA) and Ca^{2+}.[33] Furthermore, PEG (and/or EDA) can combine with Ca^{2+} (and/or CO_3^{2-}) and easily absorb on the surface of a $CaCO_3$ crystal. Therefore, $CaCO_3$ could be formed through the following reactions.

$$\text{PEG (and/or EDA)} + Ca^{2+} \rightarrow \text{PEG-}Ca^{2+}\text{ (and/or EDA-}Ca^{2+}\text{) (complex)} \quad (5)$$

$$\text{PEG (and/or EDA)} + CO_3^{2-} \rightarrow \text{PEG-}CO_3^{2-}\text{ (and/or EDA-}CO_3^{2-}\text{) (complex)} \quad (6)$$

$$\text{PEG-}Ca^{2+}\text{ (and/or EDA-}Ca^{2+}\text{)} + \text{PEG-}CO_3^{2-}\text{ (and/or EDA-}CO_3^{2-}\text{)} \rightarrow CaCO_3 + \text{PEG (and/or EDA)} \quad (7)$$

After CO_2, PEG and EDA were released from the decomposing CO_2SM; PEG, EDA, and calcium precursor solution might aggregate in PEG and EDA aqueous solution (Figure S11) as in eq 5.[33,49−52] When the surface of $CaCO_3$ crystal adsorbed PEG, which may include EDA, activities of the crystal were greatly suppressed; the free CO_2 (aq) and formed CO_3^{2-} would be trapped to form aggregates because of their electrostatic interactions, as shown in eq 6.[53] Thus, the electrostatic localization of CO_3^{2-} caused the increase of Ca^{2+} local concentration in the solution.[54,55] Additionally, Ca^{2+} could diffuse and aggregate to form a calcium-ion-concentrated area via the binding between the Ca^{2+} and PEG/or EDA, resulting in the formation of complex aggregates. According to crystal growth kinetics, when the crystal absorbs PEG and/or EDA on same surface, the crystal growth rate in same certain direction would be slowed down, leading to an isotropic growth of the crystal. Therefore, the concentration of CO_2SM was crucial in the $CaCO_3$ crystallization process because it was directly related to the concentration of PEG and EDA. Along the reaction (Figure 10, step A), the aggregates underwent heterogeneous nucleation and crystallization to from $CaCO_3$ preliminary nanoparticles at the early stage of eq 7 and Figure 10, in which preliminary $CaCO_3$ nanoparticles were composed of many aggregation molecules and behaved specifically in the reaction system.[56,57] Therefore, the preliminary aggregation particles could undergo further preferable self-assembly to form aggregated flake or pancake structures to reduce the total surface energy (Figure 10, step B). With further mineralization, these flake or pancake units could undergo further assembly into decussate structures (Figure 10, step C), then nearly spherical structures (Figure 10, steps D and E), and finally complete spheres with rough surfaces (Figure 10, step F). Therefore, according to the formation mechanism of porous $CaCO_3$, the molecular aggregation and absorption behavior in the CO_2SM aqueous solution system could induce the formation of hierarchical and porous $CaCO_3$ structures.

3.6. Circular Preparation of $CaCO_3$ Microspheres. The filtrate without $CaCO_3$ precipitate containing EDA and PEG and/or their derivates was reused to absorb CO_2. After the adsorption of CO_2, an appropriate amount $Ca(OH)_2$ solution was added into the absorbent system to prepare $CaCO_3$ microspheres. The $CaCO_3$ microspheres were smoothly produced at 90 °C within 2 h after five successive absorption−preparation cycles. Each sample was characterized with SEM and FTIR (Figure 11 and Figure S13). The experimental results showed that all $CaCO_3$ particles have the same vaterite phase. The filtered solution without $CaCO_3$ precipitate could not only be repeatedly used to absorb CO_2 but also repeatedly produced $CaCO_3$ microspheres after the bubbling of CO_2 through the CO_2SM aqueous solution.

4. CONCLUSIONS

The $CaCO_3$ microspheres with a layered nanostructure surface and a remarkable porous structure were synthesized with CO_2SM without any templates and additives, using CO_2SM as CO_2 source and $Ca(OH)_2$-saturated limpid solution. Morphologies and phase composition of the as-produced $CaCO_3$ crystals could be adjusted through crystallization conditions, such as reaction temperature and CO_2SM concentration. PEG and/or EDA and their absorption behavior in reaction system could be similar to that of surfactant, which could be an efficient template to tune the crystallization of $CaCO_3$ in the same growing direction. Additionally, in the synthesis process, EDA played an important role to adjust the pH of the reaction system, and PEG could be considered as a cosolvent to mediate the crystallization behavior of $CaCO_3$. The aggregation self-assembly of Ca^{2+} and PEG (and/or EDA) generated $CaCO_3$ microspheres with hierarchical and porous structures. Moreover, the filtered solution without $CaCO_3$ precipitates could not only be reused to absorb CO_2 but also to produce $CaCO_3$ microspheres repeatedly after the bubbling of CO_2. Therefore, this synthesis method could potentially be optimized as a new CCU technology to smoothly prepare many mineral composites with specific porosity and unique structural features.

DOI: 10.1021/acsami.5b03568
ACS Appl. Mater. Interfaces 2015, 7, 15918−15927

■ ASSOCIATED CONTENT

Supporting Information

Thirteen additional figures. The Supporting Information is available free of charge on the ACS Publications website at DOI: 10.1021/acsami.5b03568.

■ AUTHOR INFORMATION

Corresponding Author

*Tel.: +86-471-6575722. Fax: +86-471-6575722. E-mail: tadzhang@pku.edu.cn.

Notes

The authors declare no competing financial interest.

■ ACKNOWLEDGMENTS

This work was supported by the National Natural Science Foundation of China (21166017), the Research Fund for the Doctoral Program of Higher Education of China (20111514120002), the Inner Mongolia Science and Technology Key Projects, the Program for Grassland Excellent Talents of Inner Mongolia Autonomous Region, Program for New Century Excellent Talents in University (NCET-12-1017), and the Inner Mongolia Talented People Development Fund.

■ REFERENCES

(1) Sculley, J. P.; Zhou, H. C. Enhacing Amine-Supported Materials for Ambient Air Capture. *Angew. Chem., Int. Ed.* **2012**, *51*, 12660−12661.

(2) Rochelle, G. T. Amine Scrubbing for CO_2 Capture. *Science* **2009**, *325*, 1652−1654.

(3) Goeppert, A.; Czaun, M.; Surya Prakash, G. K.; Olah, G. A. Air as the Renewable Carbon Source of the Future: An Overview of CO_2 Capture from the Atmosphere. *Energy Environ. Sci.* **2012**, *5*, 7833−7853.

(4) MacDowell, N.; Florin, N.; Buchard, A.; Hallett, J.; Galindo, A.; Jackson, G.; Adjiman, C. S.; Williams, C. K.; Shah, N.; Fennell, P. An Overview of CO_2 Capture Technologies. *Energy Environ. Sci.* **2010**, *3*, 1645−1669.

(5) Zhou, S.; Chen, X.; Nguyen, T.; Voice, A. K.; Rochelle, G. T. Aqueous Ethylenediamine for CO_2 Capture. *ChemSusChem* **2010**, *3*, 913−918.

(6) Jones, C. W.; Maginn, E. J. Materials and Processes for Carbon Capture and Sequestration. *ChemSusChem* **2010**, *3*, 863−864.

(7) Patiño-Echeverri, D.; Hoppock, D. C. Reducing the Energy Penalty Costs of Postcombustion CCS Systems with Amine-Storage. *Environ. Sci. Technol.* **2012**, *46*, 1243−1252.

(8) Yang, Z. Z.; He, L. N.; Gao, J.; Liu, A. H.; Yu, B. Carbon Dioxide Utilization with C-N Bond Formation: Carbon Dioxide Capture and Subsequent Conversion. *Energy Environ. Sci.* **2012**, *5*, 6602−6639.

(9) D'Alessandro, D. M.; Smit, B.; Long, J. R. Carbon Dioxide Capture: Prospects for New Materials. *Angew. Chem., Int. Ed.* **2010**, *49*, 6058−6082.

(10) Hasib-ur-Rahman, M.; Larachi, F. CO_2 Capture in Alkanolamine-RTIL Blends via Carbamate Crystallization Route to Efficient Regeneration. *Environ. Sci. Technol.* **2012**, *46*, 11443−11450.

(11) Shang, J. P.; Liu, S. M.; Ma, X. Y.; Lu, L. J.; Deng, Y. Q. A New Route of CO_2 Catalytic Activation: Syntheses of *N*-Substituted Carbamates from Dialkyl Carbonates and Polyureas. *Green Chem.* **2012**, *14*, 2899−2906.

(12) Hwang, E. T.; Gang, H.; Chung, J.; Gu, M. B. Carbonic Anhydrase Assisted Calcium Carbonate Crystalline Composites as A Biocatalyst. *Green Chem.* **2012**, *14*, 2216−2220.

(13) Vinoba, M.; Lim, K. S.; Lee, S. H.; Jeong, S. K.; Alagar, M. Immobilization of Human Carbonic Anhydrase on Gold Nanoparticles Assembled onto Amine/Thiol-Functionalized Mesoporous SBA-15 for Biomimetic Sequestration of CO_2. *Langmuir* **2011**, *27*, 6227−6234.

(14) Mirjafari, P.; Asghari, K.; Mahinpey, N. Investigating the Application of Enzyme Carbonic Anhydrase for CO_2 Sequestration Purpose. *Ind. Eng. Chem. Res.* **2007**, *46*, 921−926.

(15) Song, D. S.; Lee, Y. C.; Park, S. B.; Han, J. I. Gaseous Carbon Dioxide Conversion and Calcium Carbonate Preparation by Magnesium Phyllosilicate. *RSC Adv.* **2014**, *4*, 4037−4040.

(16) Schenk, A. S.; Cantaert, B.; Kim, Y.-Y.; Li, Y.; Read, E. S.; Semsarilar, M.; Armes, S. P.; Meldrum, F. C. Systematic Study of the Effects of Polyamines on Calcium Carbonate Precipitation. *Chem. Mater.* **2014**, *26*, 2703−2711.

(17) Vinoba, M.; Bhagiyalakshmi, M.; Grace, A. N.; Chu, D. H.; Nam, S. C.; Yoon, Y.; Yoon, S. H.; Jeong, S. K. CO_2 Absorption and Sequestration as Various Polymorphs of $CaCO_3$ Using Sterically Hindered Amine. *Langmuir* **2013**, *29*, 15655−15663.

(18) Vinoba, M.; Bhagiyalakshmi, M.; Choi, S. Y.; Park, K. T.; Kim, H. J.; Jeong, S. K. Harvesting $CaCO_3$ Polymorphs in Situ CO_2 Capture Process. *J. Phys. Chem. C* **2014**, *118*, 17556−17566.

(19) Song, R. Q.; Colfen, H.; Xu, A. W.; Hartmann, J.; Antonietti, M. Polyelectrolyte-Directed Nanoparticle Aggregation: Systematic Morphogenesis of Calcium Carbonate by Nonclassical Crystallization. *ACS Nano* **2009**, *3*, 1966−1978.

(20) Liu, Y. D.; Goebl, J.; Yin, Y. D. Templated Synthesis of Nanostructured Materials. *Chem. Soc. Rev.* **2013**, *42*, 2610−2653.

(21) Nypelo, T.; Osterberg, M.; Laine, J. Tailoring Surface Properties of Paper Using Nanosized Precipitated Calcium Carbonate Particles. *ACS Appl. Mater. Interfaces* **2011**, *3*, 3725−3731.

(22) Yao, H. B.; Ge, J.; Mao, L. B.; Yan, Y. X.; Yu, S. H. 25th Anniversary Article: Artificial Carbonate Nanocrystals and Latered Structural Nanocomposites Inspired by Nacre: Synthesis, Fabrication and Applications. *Adv. Mater.* **2014**, *26*, 163−188.

(23) Barhoum, A.; Rahier, H.; Abou-Zaied, R. E.; Rehan, M.; Dufour, T.; Hill, G.; Dufresne, A. Effect of Cationic and Anionic Surfactants on the Application of Calcium Carbonate Nanoparticles in Paper Coating. *ACS Appl. Mater. Interfaces* **2014**, *6*, 2734−2744.

(24) Gu, F. B.; Wang, Z.; Han, D.; Guo, G.; Guo, H. Crystallization of Rare Earth Carbonate Nanostructures in the Reverse Micelle System. *Cryst. Growth Des.* **2007**, *7*, 1452−1458.

(25) Asenath-Smith, E.; Li, H. Y.; Keene, E. C.; Seh, Z. W.; Estroff, L. A. Crystal Growth of Calcium Carbonate in Hydrogels as A Model of Biomineralization. *Adv. Funct. Mater.* **2012**, *22*, 2891−2914.

(26) Liang, X. H.; Xiang, J. H.; Zhang, F. S.; Xing, L.; Song, B.; Chen, S. W. Fabrication of Hierarchical $CaCO_3$ Mesoporous Spheres: Particle-Mediated Self-Organization Induced by Biphase Interfaces and SAMs. *Langmuir* **2010**, *26*, 5882−5888.

(27) Gao, Y. X.; Yu, S. H.; Cong, H. P.; Jiang, J.; Xu, A. W.; Dong, W. F.; Colfen, H. Block-Copolymer-Controlled Growth of $CaCO_3$ Microrings. *J. Phys. Chem. B* **2006**, *110*, 6432−6436.

(28) Chen, S. F.; Zhu, J. H.; Jiang, J.; Cai, G. B.; Yu, S. H. Polymer-Controlled Crystallization of Unique Mineral Superstructures. *Adv. Mater.* **2010**, *22*, 540−545.

(29) Guo, X. H.; Yu, S. H.; Cai, G. B. Crystallization in A Mixture of Solvents by Using A Crystal Modifier: Morphology Control in the Synthesis of Highly Monodisperse $CaCO_3$ Microspheres. *Angew. Chem., Int. Ed.* **2006**, *45*, 3977−3981.

(30) Zhao, T. X.; Guo, B.; Han, L. M.; Zhu, N.; Gao, F.; Li, Q.; Li, L. H.; Zhang, J. B. CO_2 Fixation into Novel CO_2 Storage Materials Composed of 1,2-Ethanediamine and Ethylene Glycol Derivatives. *ChemPhysChem* **2015**, DOI: 10.1002/cphc.201500206.

(31) Kontoyannis, C. G.; Vagenas, N. V. Calcium Carbonate Phase Analysis Using XRD and FT-Raman Spectroscopy. *Analyst* **2000**, *125*, 251−255.

(32) Sarkar, A.; Dutta, K.; Mahapatra, S. Polymorph Control of Calcium Carbonate Using Insoluble Layered Double Hydroxide. *Cryst. Growth Des.* **2013**, *13*, 204−211.

(33) Xu, X. Y.; Zhao, Y.; Lai, Q. Y.; Hao, Y. J. Effect of Polyethylene Glycol on Phase and Morphology of Calcium Carbonate. *J. Appl. Polym. Sci.* **2011**, *119*, 319−324.

(34) Jiang, J. X.; Ye, J. Z.; Zhang, G. W.; Gong, X. H.; Nie, L. H.; Liu, J. N. Polymorph and Morphology Control of $CaCO_3$ via Temperature

and PEG During the Decomposition of $Ca(HCO_3)_2$. *J. Am. Ceram. Soc.* **2012**, *95*, 3735−3738.
(35) Chuajiw, W.; Takatori, K.; Igarashi, T.; Hara, H.; Fukushima, Y. The Influence of Aliphatic Amines, Aiamines, and Amino Acids on the Polymorph of Calcium Carbonate Precipitated by the Introduction of Carbon Dioxide Gas into Calcium Hydroxide Aqueous Suspensions. *J. Cryst. Growth* **2014**, *386*, 119−127.
(36) Zheng, L.; Hu, Y. L.; Ma, Y. J.; Zhou, Y.; Nie, F. D.; Liu, X.; Pei, C. H. Egg-White-Mediated Crystallization of Calcium Carbonate. *J. Cryst. Growth* **2012**, *361*, 217−224.
(37) Zhou, G. T.; Yu, J. C.; Wang, X. C.; Zhang, L. Z. Sonochemical Synthesis of Aragonite-Type Calcium Carbonate With Different Morphologies. *New J. Chem.* **2004**, *28*, 1027−1031.
(38) Kirboga, S.; Oner, M.; Akyol, E. The Effect of Ultrasonication on Calcium Carbonate Crystallization in the Presence of Biopolymer. *J. Cryst. Growth* **2014**, *401*, 266−270.
(39) Wang, H.; Alfredsson, V.; Tropsch, J.; Ettl, R.; Nylander, T. Formation of $CaCO_3$ Deposits on Hard Surfaces-Effect of Bulk Solution Conditions and Surface Properties. *ACS Appl. Mater. Interfaces* **2013**, *5*, 4035−4045.
(40) Cheng, B.; Lei, M.; Yu, J. G.; Zhao, X. J. Preparation of Monodispersed Cubic Calcium Carbonate Particles via Precipitation Reaction. *Mater. Lett.* **2004**, *58*, 1565−1570.
(41) Sheng, Y.; Zhao, J. Z.; Zhou, B.; Ding, X. F.; Deng, Y. H.; Wang, Z. C. In Situ Preparation of $CaCO_3$/Polystyrene Composite Nanoparticles. *Mater. Lett.* **2006**, *60*, 3248−3250.
(42) He, Z. Q.; Liu, J. R.; Zhang, J. B.; Zhang, N. Spectroscopic Study on the Intermolecular Interaction of SO_2 Absorption in Poly-Ethylene Glycol + H_2O Systems. *Korean J. Chem. Eng.* **2014**, *31*, 514−521.
(43) Brisdon, B. J.; Heywood, B. R.; Hodson, A. G. W.; Mann, S.; Wong, K. K. W. Polymer-Mediated Crystallization of Inorganic Solids: Calcite Nucleation on Poly (Organosiloxane) Surfaces. *Adv. Mater.* **1993**, *5*, 49−51.
(44) Guo, X. H.; Xu, A. W.; Yu, S. H. Crystallization of Calcium Carbonate Mineral with Hierarchical Structures in DMF Solution Under Control of Poly (Ethylene Glycol)-b-Poly (L-Glutamic Acid): Effects of Crystallization Temperature and Polymer Concentration. *Cryst. Growth Des.* **2008**, *8*, 1233−1242.
(45) Liu, L.; Jiang, J.; Yu, S. H. Polymorph Selection and Structure Evolution of $CaCO_3$ Mesocrystals Under Control of Poly (Sodium 4-Styrenesulfonate): Synergetic Effect of Temperature and Mixed Solvent. *Cryst. Growth Des.* **2014**, *14*, 6048−6056.
(46) Xiao, J. W.; Yang, S. H. Hollow Calcite Crystals with Complex Morphologies Formed From Amorphous Precursors and Regulated by Surfactant Micellar Structures. *CrystEngComm* **2010**, *12*, 3296−3304.
(47) Zhao, D. Zhou.; Jiang, J. H.; Xu, J. N.; Yang, L.; Song, T. Y.; Zhang, P. Synthesis of Template-Free Hollow Vaterite $CaCO_3$ Microspheres in the H_2O/EG System. *Mater. Lett.* **2013**, *104*, 28−30.
(48) Zhao, Y. Y.; Li, S. X.; Yu, L.; Liu, Y. H.; Wang, X. Q.; Jiao, J. J. The preparation of Calcium Carbonate Caystals Regulated Mixed Cationic/Cationic Surfactants. *J. Cryst. Growth* **2011**, *324*, 278−283.
(49) Mihai, M.; Schwarz, S.; Doroftei, F.; Simionescu, B. C. Calcium Carbonate/Polymers Moiroparticles Tuned by Complementary Polyelectrolytes as Complex Macromolecular Templates. *Cryst. Growth Des.* **2014**, *14*, 6073−6083.
(50) Qi, R. J.; Zhu, Y. J. Microwave-Assisted of Calcium Carbonate (vaterite) of Various Morphologies in Water-Ethylene Glycol Mixed Solvents. *J. Phys. Chem. B* **2006**, *110*, 8302−8306.
(51) Li, Z. Q.; Xiong, Y. J.; Xie, Y. Selected-Control Synthesis of ZnO Nanowires and Nanorods via A PEG-Assisted Route. *Inorg. Chem.* **2003**, *42*, 8105−8109.
(52) El-Sheikh, S. M.; El-Sherbiny, S.; Barhoum, A.; Deng, Y. Effects of Cationic Surfactant During the Precipitation of Calcium Carbonate Nano-Particles on Their Size, Morphology, and Other Characteristics. *Colloids Surf., A* **2013**, *422*, 44−49.
(53) Zhao, Y.; Chen, Z. H.; Wang, H. Y.; Wang, J. J. Crystallization Control of $CaCO_3$ by Ionic Liquids in Aqueous Solution. *Cryst. Growth Des.* **2009**, *9*, 4984−4986.
(54) Barhoum, A.; Van Assche, G. V.; Makhlouf, A. S. H.; Terryn, H.; Baert, K.; Delplancke, M. P.; El-Sheikh, S. M.; Rahier, H. A green, Simple Chemical Route for the Synthesis of Pure Nanocalcite Crystals. *Cryst. Growth Des.* **2015**, *15*, 573−580.
(55) El-Sheikh, S.; Barhoum, A.; El-Sherbiny, S.; Morsy, F.; ElMidany, A.; Rahier, H. Preparation of Superhydrophobic Nano-calcite Crystals Using Box-Behnken Design. *Arabian J. Chem.* **2014**, n/a DOI: 10.1016/j.arabjc.2014.11.003.
(56) Guo, X. H.; Liu, L.; Wang, W.; Zhang, J.; Wang, Y.; Yu, S. H. Controlled Crystallization of Hierarchical and Porous Calcium Carbonate Crystals Using Polypeptide Type Block Copolymer as Crystal Growth Modifier in A Mixed Solution. *CrystEngComm* **2011**, *13*, 2054−2061.
(57) Geng, X.; Liu, L.; Jiang, J.; Yu, S. H. Crystallization of $CaCO_3$ Mesocrystals and Complex Aggregates in A Mixed Solvent Media Using Polystyrene Sulfonate as A Crystal Growth Modifier. *Cryst. Growth Des.* **2010**, *10*, 3448−3453.

DOI: 10.1021/acsami.5b03568
ACS Appl. Mater. Interfaces 2015, 7, 15918−15927